LAWRENCE
LIVERMORE
NATIONAL
LABORATORY

LLNL-JRNL-653840

Electrical properties of methane hydrate + sediment mixtures

W. L. Du Frane, L. A. Stern, S. Constable, K. A. Weitemeyer, M. M. Smith, J. J. Roberts

April 29, 2014

Journal of Geophysical Research Solid Earth

Disclaimer

Introduction

Gas hydrates are clathrate structures of H_2O that encage gases of small molecular diameter, such as methane, ethane, propane, CO_2, etc. [*Sloan and Koh,* 2007]. The formation of gas hydrates typically requires moderately low temperatures, high pressure, and sufficient quantities of water and free- or dissolved-phase hydrate-forming gas. Such conditions occur globally – and often extensively – in permafrost regions and shallow marine environments such as in seafloor sediments along continental margins [*Kvenvolden and Lorenson,* 2001]. Consequently, gas hydrates are very common in these regions and harbor a significant hydrocarbon source that is of keen interest for economic as well as geohazard considerations [e.g., *Kvenvolden,* 1999*; Collett,* 2002*; Ruppel,* 2007*, Maslin et al.,* 2010*, Boswell and Collett,* 2011]. Estimates of the total global hydrate inventory have varied by up to four orders of magnitude [e.g., *Kvenvolden, 1999; Milkov, 2004*], with more recent estimates predicting that the amount of carbon bound by gas hydrates is greater than the total amounts in the atmosphere plus conventional natural gas reserves [*Boswell and Collett,* 2011*; Wallman et al.,* 2012]. Estimates continue to improve with significant advances in global modeling and geophysical mapping of gas hydrate inventories [*Maslin et al.,* 2010*; Boswell and Collett,* 2011].

Traditional methods for geophysical detection of gas hydrates include well-logging and seismic surveys. Well-logging provides point measurements of gas hydrate concentration versus depth, but is expensive and invasive. Seismic methods are also used to map the spatial distribution of gas hydrate deposits. The presence of a bottom simulating reflector (BSR) may indicate the phase boundary between gas hydrate and free gas [e.g., *Hornbach et al.,* 2003]. This boundary alone, however, provides little information about the amount and distribution of gas hydrate above it. Seismic blanking zones can be used in some cases to help predict gas hydrate

54 occurrence [e.g., *Hornbach et al.*, 2003; *Zhang and McMechan*, 2006]. Additional geophysical
55 methods are clearly needed to obtain a more complete picture of gas hydrate distribution.
56 Electrical methods can be effective in remotely detecting gas hydrate due to the
57 sensitivity of electrical properties to the compositions and microstructures of sedimentary
58 materials [*Edwards*, 1997]. Gas hydrates have low electrical conductivity (σ – note that this is
59 the inverse of resistivity: $\rho = \sigma^{-1}$) that provides a suitable target for marine controlled source
60 electromagnetic (CSEM) surveys. CSEM sounding measures the amplitude and phase of
61 electromagnetic (EM) energy through the seafloor at one or more frequencies, and this data can
62 be inverted to obtain the spatial distribution of conductivity. The combined use of both seismic
63 and EM methods can help distinguish between gas (low velocity, high resistivity) and gas
64 hydrate (high velocity, high resistivity), to mapboth the upper and lower boundaries of gas
65 hydrate deposits. Pilot CSEM studies have demonstrated the sensitivity of this method in
66 assessing general gas hydrate concentration, saturation, and distribution patterns [e.g.
67 *Schwalenberg et al.*, 2005; *Evans*, 2007; *Weitemeyer et al.*, 2006, 2011]. Quantifying the
68 estimates of hydrate volume, however, requires knowledge of the electrical conductivity of gas
69 hydrates in combination with petrophysical mixing relations established from theory and
70 experiment [*Collett and Ladd*, 2000; *Ellis et al.*, 2008].
71 Several previous laboratory studies focused on the electrical properties of gas hydrates in
72 mixtures with sediment and water [*Spangenberg and Kulenkampff*, 2006*; Lee et al.*, 2010; *Ren et*
73 *al*, 2010]. The electrical conductivity of CH_4 hydrate was measured during formation from liquid
74 water in the pore space of glass beads [*Spangenberg and Kulenkampff*, 2006] and quartz sand
75 [*Ren et al.*, 2010]. A similar study examined electrical conductivity before and after gas hydrate
76 formation within sandy sediments, using brine with 3.35 wt% NaCl [*Li et al.*, 2012]. These

measurements are important for helping resolve mixing laws, but they are dominated by the presence of water, which obscures quantitative information on the more subtle contributions by gas hydrate or sediments to the overall electrical conductivity. Geometrical mixing laws, such as Archie's law or Hashin-Shtrikman lower bounds models can be used with the assumption that gas hydrate has low σ compared to the surrounding seawater [*Archie,* 1942; *Hashin and Shtrikman,* 1962; *Glover et al.,* 2000]. This assumption is valid when the conductive pore water phase dominates the bulk conductivity – which is in fact the common mode in nature – but may not be valid where gas hydrate (the low conductivity phase) occurs in massive form or otherwise dominates bulk conductivity. The latter case can be especially important for mapping hydrate formations that are impermeable to gas, as they may also be relatively impermeable to pore water [e.g., *Kneafsey et al.,* 2011]. *Lee et al.* [2010] published a systematic examination of electrical conductivity and permittivity (electric field response) for water-free tetrahydrofuran (THF) hydrate mixed with sand, silts, and clay, but as THF hydrate is only an analog for natural gas hydrate, it may have different conduction mechanisms due to its different molecular structure as a structure II (sII) hydrate versus the more common naturally occurring structure I (sI) hydrate.

Lastly, the previous studies have not carefully examined the temperature dependence of the electrical conductivity gas hydrate/sediment mixtures. Most electrical insulators, such as gas hydrates, have electrical conductivity that increases exponentially with increasing temperature. Details of this relationship can yield important mechanistic information about conduction mechanisms [e.g., *Roberts,* 2002], which must be understood to properly apply laboratory measurements to the widely varying conditions that exist in the field.

Du Frane et al. [2011] recently published the first direct measurements of the electrical conductivity of single-phase CH_4 hydrate formed from reacting high purity H_2O and CH_4. The σ

of CH_4 hydrate ranged between 10^{-5} to 10^{-4} S/m for temperatures between -15 and 15 °C, indicating strong, positive temperature dependence. These results were obtained in a custom-built pressure cell designed to allow synthesis of increasingly complex gas hydrate + sediment ± water mixtures, in which electrical conductivity can be measured *in situ* during both formation and dissociation of the hydrate phase. This method allows for controlled and pre-determined mixing and textural arrangement of the various components in the system, meaning that the effects of individual components can be assessed for better integration into mixing models. In this study, we present new electrical conductivity results for the 2-component system of fully reacted (i.e. water-free) methane hydrate in mixtures with varying proportions of sediments (quartz sand and glass beads) for a range of temperatures between -15 to 15 °C.

We note that many – if not most – gas hydrate systems in nature contain a pore water component that dominates the overall electrical properties of the system, hence results from multi-component samples that include a pore water phase will obviously be critical for modeling most systems in nature. However, massive gas hydrate formations that are lacking in pore water are expected to be present in some locations in nature, and such units could be of high economic value. Measuring electrical conductivity of mixed-phase systems in which there is no knowledge of the competing effects of the separate components, how the various components are positioned or connected within the system, or in what manner individual conduction mechanisms influence total conductivity, would simply yield isolated and ambiguous measurements due to the numerous unknowns. Also, the more subtle effects of adding sediment to gas hydrate would be eclipsed when adding an additional free water phase, and the only way to investigate such effects is by careful measurement of liquid-free systems. Future experiments are anticipated to

incorporate a free water phase into the system in order to help develop the more complex models relevant to most natural systems.

Experimental Techniques

We developed a cell to synthesize gas hydrate and simultaneously measure electrical conductivity (Fig. 1). The apparatus is built around a commercially available pressure vessel (High Pressure Equipment Company) with the addition of high pressure manifolds on each end-cap. Each manifold has a single port feed-through where methane gas and electrical leads enter into the vessel. Samples were 2.0" in diameter and 0.5" thick, and were sandwiched by silver electrodes and Teflon spacers. Methane hydrate was synthesized in the pressure cell using a temperature cycling technique that enables full reaction of H_2O ice "seeds" and pressurized CH_4 (15-30 MPa) to polycrystalline CH_4 hydrate in a reproducible manner [*Stern et al.*, 1996, 2004]. The reactant ice seeds were made from a block of nearly gas-free ice that was grown from distilled-deionized water, then crushed and sieved to 0.180-0.250 mm.

Starting samples were prepared from granular ice that was free of sediment, mixed with quartz sand, or mixed with silica glass beads. The OK#1 sand and glass beads were not washed prior to use. Mixtures were made in proportions ranging from pure (100 %) ice down to 10 vol% ice, and 0-90 vol% sand or beads, with percentages referring to the solid phase only. All samples initially contained ~30-40% porosity, determined from mass measurements of each phase prior to mixing and packing into the known-volume sample chamber. Ice-only samples had highest initial porosity given their relatively uniform grain size compared to mixed-phase samples. In all samples, porosity reduces during reaction due to the ~ 16% volumetric increase of the H_2O phase that accompanies the ice to hydrate reaction, assuming density of ice and an empty sI hydrate lattice to be 917 and 790 kg/m3 respectively [*Dvorkin et al.*, 2000]. Porosity of final

samples is thus easily calculated, and the issue of porosity has been discussed previously in *Du Frane et al.* [2011]. For mixtures with sand, we used Oklahoma #1 (OK #1) high-purity quartz (SiO_2) sand that had minor hematite, illite, calcite, and alumina (< 1 vol % combined), and a narrow grain size distribution with 84% of grain diameters between 0.106 to 0.250 mm [*Durham et al.*, 2009]. Two sample mixtures contained glass beads (Cataphote) made of high-purity soda-lime-silica (amorphous SiO_2 with a small amount of Na_2CO_3 [*NIIR Board of Consultants & Engineers*, 2005]) glass with diameters ranging between 0.105 to 0.125 mm. Sample mixtures and run conditions are listed in Table 1.

The cell was first loaded with seed ice ± sediments and placed under methane pressure in a temperature controlled bath of inert coolant, d-Limonene. Heating the reactants above the ice point to conditions well within the methane hydrate stability field promoted full and efficient reaction to hydrate. The first run was carried out with one manifold replaced by a thermocouple, to calibrate and monitor the synthesis reaction; any unreacted H_2O remaining after the heating stage was easily discernible by a discontinuity in the pressure-temperature curve upon cooling the sample below the ice point, in which case additional heating cycles were implemented. Subsequent runs were then performed without a thermocouple in the sample, using the σ measurement itself as an indicator of complete reaction, as it was similarly sensitive to excess liquid when cycling past the freezing/melting point. Samples were cycled multiple (≥7) times to ensure full reaction. During experiments, temperature and electrical conductivity were monitored and recorded throughout formation, stabilization, and dissociation.

Impedance spectroscopy data (20 Hz to 2 MHz) were collected with an Agilent E4980A LCR (inductance, capacitance, and resistance) meter throughout each run. The spectra were used to determine what frequency impedance measurement is needed to calculate the true electrical

conductivity of the sample while excluding systemic contributions [*e.g. Roberts et al.*, 1991; 1993]. It should be noted that the range of frequencies swept during impedance spectroscopy measurements in the lab are unrelated to the frequencies used in CSEM field measurements. Our previous equivalent circuit modeling [*Du Frane et al.*, 2011] indicates that conductivity can be measured reliably at the frequency associated with the smallest capacitance to isolate the electrical response of our samples and avoid systemic effects, such as electrode polarization at low frequency. Measurements were performed on samples with fully-reacted CH_4 hydrate between -15 to 15 °C after 7 or more automated temperature cycles. Heating was isochoric such that the pore pressure of CH_4 gas increased during the measurement (pressure ranges are listed in Table 1). Comparative impedance measurements were also performed between -15 to -2 °C on several samples after the CH_4 hydrate was dissociated back into ice by venting CH_4 from the vessel at temperatures ≤ -3 °C for ≥ 6 days (Table 1). Single frequency electrical conductivity (typically at 100 kHz) was monitored during CH_4 hydrate synthesis and dissociation to verify completion of each reaction. We also monitored sample conductivity after each incremental heating step to ensure that samples had re-equilibrated to each new temperature before performing broad-band measurements used to calculate electrical conductivity.

Samples containing either CH_4 hydrate or ice were recovered for cryogenic scanning electron microscope (cryo-SEM) analysis. To recover samples with CH_4 hydrate, the vessel was cooled sufficiently with liquid nitrogen (LN) prior to depressurization. CH_4 hydrate samples were then stored and transported in LN to a cryo-preparation station and imaging stage (Gatan Alto Model 2100) that in turn attached directly to a LEO982 field emission SEM. Samples were cleaved under vacuum in the preparation station to produce fresh surfaces uncontaminated by water condensation, and then transferred under vacuum into the SEM column. A thermocouple

191 embedded in the SEM sample stage recorded temperature throughout the imaging process.
192 Imaging was conducted at temperature < -185 °C, vacuum < 10^{-6} kPa, and accelerating voltage ≤
193 2 kV. Further details of cryo-SEM imaging techniques and instrumentation are given in *Stern et*
194 *al.* [2004]. Sample material was destroyed in the process of SEM imaging due to the high
195 vacuum environment.

196 **Results**

197 ***Cryogenic scanning electron microscopy***

198 Cryo-SEM images verified that the synthesized gas hydrate was fully-reacted
199 polycrystalline CH_4 hydrate (Fig. 2). Sample porosity is greatly reduced in the final material due
200 to the volumetric increase accompanying the ice to gas hydrate reaction, resulting in primarily
201 isolated macro-pores (Fig. 2A). Images verified that grain-scale characteristics were in general
202 reproducible across all samples, with individual grains ranging from 10-80 μm in diameter. CH_4
203 hydrate grains were fully dense as grown (Fig. 2A and inset), but surface pitting developed
204 within several minutes of imaging in the high-vacuum column (Fig. 2B and inset). OK#1 and
205 glass bead sediments were uniformly distributed in mixed samples (Fig 2C-F), thereby
206 establishing a basis for comparison of σ measurements between mixed-phase runs. Despite
207 annealing of ice grains accompanying dissociation, SEM images also indicated no significant
208 migration of sediments during any given run, thus enabling comparison of σ measurements
209 before, during, and after dissociation within a single run. The hydrate or ice grains appear to be
210 well connected in all samples except for the one with 10:90 vol% ice:sand (Fig. 2F). We were
211 unable to evaluate subtle textural changes due to the effects of sublimation during cryo-SEM
212 analyses. It has been previously established that our formation techniques result in samples with
213 consistent texture, having undergone multiple cycles through the ice point with lengthy holds at

the peak temperatures well above 0°C that allows samples to anneal [*Stern et al.*, 2004]. The texture of the methane hydrate in samples mixed with sand also resembles textures observed in at least some hydrate-bearing sands retrieved from nature, such as from the Alaska North Slope [*Stern et al.*, 2011].

Electrical Conductivity

The H_2O was verified to be fully-reacted to CH_4 hydrate within several temperature cycles, consistent with previous studies [e.g., *Stern et al.*, 1996; 2004]. Impedance spectra were then collected on samples while heating incrementally from -15 to 15 °C, with samples undergoing 7-16 temperature cycles total during the full run (Table 1). At each temperature increment, samples typically required ~1 hour to re-equilibrate before electrical conductivity could be measured due to the low thermal conductivity/ diffusivity of the samples [e.g., *Waite et al., 2007*].

The addition of sediment complicated the interpretation of impedance spectra of the CH_4 hydrate. Equivalent circuit modeling of these spectra was not feasible due to the noisiness of impedance magnitude data measured at frequencies > 500 kHz and < 1 kHz (Fig. 3A). Equivalent circuit modeling by *Du Frane et al.* [2011] for sediment-free samples indicated that the impedance magnitude associated with the maximum phase angle could be used to avoid systemic effects due to the electrodes and their leads (see Fig. 3A in *Du Frane et al.* [2011]). For CH_4 hydrate mixed with sediments, the phase angle data show maxima at intermediate frequencies on the order of ~100 kHz similar to pure CH_4 hydrate samples (Fig. 3B). This was also the case after dissociation of CH_4 hydrate to ice (Fig. 3C and 3D). Based on these observations, we similarly used phase angle to determine the correct frequency to calculate electrical conductivity.

237 Electrical conductivity of mixtures generally exhibited exponential dependence on
238 temperature both after CH_4 hydrate formation, and after dissociation to ice, which is typical for
239 electrolytic materials. We fit data using an Arrhenius expression,

240 $$\sigma(T) = \sigma_0 e^{-E_a/RT} \quad (1)$$

241 where σ_0 is a pre-exponential constant (S/m), E_a is activation energy (kJ/mol), R is the gas
242 constant (8.314 J/mol/K), and T is temperature (K). Plotting Log(σ) versus 10^3/T(K) gives slopes
243 that are proportional to E_a (Fig. 4). Table 1 gives fitted parameters for σ_0 and E_a for each sample
244 mixture that can be used to calculate electrical conductivity as function of temperature.
245 Increased sand concentrations of up to ~45 vol% in mixtures with CH_4 hydrate resulted in
246 increased conductivity of the overall mixtures (runs 4, 5, 6, and 8; Table 1, Fig. 4). Conversely,
247 the sample with 10:90 vol% CH_4 hydrate:sand (run 10) had much lower conductivity. SEM
248 images indicate that dissociated ice, and likely CH_4 hydrate, was poorly connected in this sample
249 (Fig. 2F), in which case surface conductivity through the well-connected sand may have a non-
250 negligible contribution to the electrical conductivity of the mixture [e.g., *Wildenschild et al.*,
251 2000; *Revil* et al., 2014]. Activation energy decreased substantially with increasing sand, from
252 30.6 kJ/mol for pure CH_4 hydrate to 7.66 kJ/mol for a sample containing ~45 vol% sand. The
253 CH_4 hydrate + sand mixtures showed little σ change as we vented CH_4 to approach the edge of
254 the stability field (Fig. 5A), indicating that the effects of pressure are small in the range of these
255 experiments. Once the CH_4 gas was fully vented, electrical conductivity slowly began to increase
256 as the CH_4 hydrate in samples dissociated to ice (Fig. 5B). The presence of sand produced
257 similar σ increases after dissociation of CH_4 hydrate to ice, but had less effect on E_a.
258 Two experiments (runs 7 and 9) were conducted using ~ 45 vol% glass beads of similar
259 grain size as OK#1 for comparison to runs with sand. Run 9 showed that glass beads had less

overall effect on electrical properties of CH_4 hydrate than sand (Fig. 4); mixing glass beads into CH_4 hydrate led to only a slight increase in overall electrical conductivity and a slight decrease in activation energy. The glass beads are less angular, and consequently will have less connectivity than sand for a given volume percentage. However, SEM images (Fig. 2C and 2E) indicate that both sand and glass beads are well-connected at ~45 vol%. Small differences in connectivity past the percolation threshold are unlikely to account for the substantially larger effects that sand has on electrical conductivity of mixtures with CH_4 hydrate relative to glass beads (Fig. 4), but further studies are needed to fully evaluate the effects of angularity and grain orientation. Ion chromatography (IC) and total inorganic carbon (TIC) analyses conducted on select samples that were dissociated after testing (runs 3, 5, 6, and 7) verified that significant amounts of ionic impurities were present on the surfaces of both the sand and glass beads (data presented in Supporting Information).

Discussion

Electrical conductivity measurements on water-free CH_4 hydrate + sediment mixtures in this study are predictably lower in magnitude than those previously reported for water-bearing mixtures [*Spangenberg and Kulenkampff* 2006; *Ren et al.*, 2010; *Li et al.*, 2012]. The σ of CH_4 hydrate with ~45 vol% quartz sand (OK#1) is 1 order of magnitude lower than a measurement of $10^{-2.42}$ S/m reported for 62 vol% glass beads packs saturated with 36 vol% CH_4 hydrate and 2 vol% water [*Spangenberg and Kulenkampff* 2006]. Measurements on sand packs saturated with ~10 vol% CH_4 hydrate and ~20 vol% water are on the order of $10^{-0.5}$ S/m at 5 °C [*Ren et al.*, 2010], significantly higher than measurements on water free mixtures.

Unexpectedly, the addition of sediment in the form of quartz sand and glass beads increased the overall electrical conductivity of most sample mixtures with CH_4 hydrate or ice

283 (Fig. 4). This is somewhat counterintuitive because quartz sand and silica beads by themselves
284 have low electrical conductivity. The one exception was the mixture with 90 vol% sand that had
285 significantly lower electrical conductivity than other sample mixtures. Ice appeared poorly
286 connected within this mixture in SEM images (Fig. 2F), suggesting that this high concentration
287 of sand exceeds the percolation threshold (i.e. the concentration required for connectivity) for
288 both the dissociated ice and CH_4 hydrate. This indicates that the CH_4 hydrate or ice grains
289 provided the primary path for current when connected through sample mixtures, although the
290 presence of sediment raised total electrical conductivity. The increase to electrical conductivity
291 by the presence of ~45 vol % glass beads was significant (run 9), but substantially lower than the
292 effects of naturally weathered quartz sand (Fig. 4).
293 Electrical conductivity was likely enhanced in the CH_4 hydrate grains by impurities that
294 were introduced from weathered surfaces of the sand. Ionic doping of the CH_4 hydrate grains
295 could explain why activation energies decreased with increased sand concentrations. The
296 activation energy contains two physical phenomena: an increase in defect mobility with
297 temperature and an increase in defect population with temperature. These impurities are likely to
298 have low mobility but are charge-compensated by protonic defects that have relatively high
299 mobility. When there are few to no impurities present, protonic defects are likely to be thermally
300 induced in the gas hydrate structure, which would make electrical conductivity strongly
301 dependent on temperature. If the structure is doped with impurities there could be a population of
302 protonic defects induced to maintain charge balance that are relatively insensitive to temperature.
303 Doping would cause electrical conductivity to increase substantially with a population of charge
304 carriers that mask those that are thermally induced, yielding electrical conductivity with less
305 temperature dependence, i.e. lower activation energy. The electrical conductivity of CH_4 hydrate

+ sand mixtures was substantially higher than pure CH_4 hydrate (Fig. 4), which indicates that some impurities from sand can be included in CH_4 hydrate. Probable candidates include ions that were found in higher concentrations on the surfaces of the sand compared with those on the surface of glass beads: K^+, Ca^{2+}, Mg^{2+}, NH_4^+, Cl^-, SO_4^{2-} (Table S1 in Supporting Information). Most impurities that are dissolved in water become excluded during ice crystallization, with the exception of a few acids (HF, HCl), ammonia (NH_3), alkalis (KOH, NaOH) and their derivatives (NH_4F or KCl) that drastically change the protonic carrier concentration [e.g., *Petrenko and Whitworth*, 1999]. KOH inclusion into THF hydrate has also been demonstrated to trigger formation of charge carriers, Bjerrum and protonic defects, and could also affect mobilities of other point defects [*Nelson et al.*, 2013]. If CH_4 hydrate behaves similar to ice, then the sand may have contributed KOH and its derivative KCl during synthesis, which is consistent with IC detection of both K^+ water melted from samples containing sand (runs 5 and 6), but not in those containing glass beads (run 7) or in those that did contain any sediment (run 3) (Table S1). It would also be expected that NaCl and Na_2CO_3 would be excluded during its crystallization. Inclusion of K^+ and Cl^- is thus one possible explanation for what caused the observed doping effect on the electrical conductivity of CH_4 hydrate-sand mixtures.

A first-order model of the doping effect on the electrical conductivity of CH_4 hydrate and ice caused by impurities from sand is presented in Supporting Information section S2. The model includes a second conductivity term that is proportional to sand concentration, and assumes a simple parallel mixing law relationship. We were able to obtain excellent fits to data for sample mixtures with 10 or 30 vol% sand, but not for those with ~45 or 90 vol% sand. This is because mixing laws are typically incapable of expressing behavior across percolation thresholds. If impurities do not move far from the sand surface, CH_4 hydrate/sand interfaces may

have higher electrical conductivity than the bulk conductivity of CH_4 hydrate grains. If both CH_4 hydrate and sand are interconnected, then interfaces between the two phases will also be interconnected possibly creating a high conductivity path throughout mixtures. This could explain the large increase in electrical conductivity and decrease in activation energy when increasing the amount of sand in mixtures from 30 to ~45 vol%. Therefore, the model is only applicable to scenarios where hydrate/ice is well connected in mixtures, but the sediment is not, and should be considered preliminary at best given the limited range of compositions examined here.

The results of this study imply that sediment composition, in addition to sediment amount and distribution, will be a critical factor in determining bulk electrical conductivity of gas hydrates, at least in sections devoid of pore water. In nature, impurities could be acquired from sediments, organic material, or pore water itself. While gas hydrate formation is typically viewed as a purification process – a promising aspect that can potentially be exploited for desalination of highly saline waste water into potable water [*Cha and Seol,* 2013] – our results suggest that even trace amounts of impurities incorporated within the CH_4 hydrate lattice produce substantial effects on the overall electrical properties of CH_4 hydrate. The OK#1 and glass beads were chosen for this study because they are regarded to have high purity in comparison to most sediment and facilitated our attempt to study the fundamental contributions of individual conduction mechanisms to total conductivity. In contrast, sediments found in permafrost and marine settings have the potential to contribute different and larger concentrations of impurities. Pore water may also contribute impurities in amounts substantial enough to affect the electrical properties, although this effect would likely be masked in comparison with the effect of the pore water itself. For example, seawater contains roughly 400 mg/L of K^+ [*Webb,* 1939], which is

within the range of measured values for water melted from the post-run samples (Table S1). Physical and chemical conditions will also play a role in what concentrations of impurities are included during gas hydrate formation. Chemical transfer of ionic impurities must be carefully considered to accurately determine the electrical conductivity of gas hydrate formations in marine sediments.

Conclusions

The electrical conductivity of liquid-free CH_4 hydrate-sediment mixtures is highly dependent on composition and temperature. Increasing sand concentrations up to 45 vol% increased the overall electrical conductivity of mixtures by as much as an order of magnitude at 0 °C. The overall electrical conductivity of mixtures plummeted in a sample containing a sufficiently high sediment concentration (90 vol%) that crossed percolation threshold, such that the CH_4 hydrate was poorly connected. This observation provides evidence that CH_4 hydrate (and ice after dissociation) is the primary current path within mixtures.

Ionic impurities from sand caused a doping effect on the electrical properties of CH_4 hydrate (and ice). This is consistent with the observation that increasing sand content in mixtures resulted in higher magnitude electrical conductivity and less temperature dependence, i.e. lower activation energy values. Over the range of geologically-relevant temperatures from -5 to 15 °C, the overall electrical conductivity of CH_4 hydrate mixtures with $\leq$ 30 vol % sand increased by ~3 times. Mixtures with $\geq$ 45 vol% CH_4 hydrate exhibited almost no change in conductivity over that same range. Most of the ionic impurities associated with the glass beads appear to have been excluded during CH_4 hydrate formation (Na^+, CO_3^{2-}, HCO_3^-), while at least some of the ionic impurities more strongly associated with the sand grains were included (K^+, Ca^{2+}, Mg^{2+}, NH_4^+, Cl^-, SO_4^{2-}).

375 The addition of sediments to samples is the methodical 2nd step in the evolution of this
376 work, following our initial measurements of pure, end-member CH_4 hydrate. While these results
377 can only be loosely applied to "dry" systems with essentially no pore water present, they are
378 necessary experiments to increase the fundamental understanding of individual conduction
379 mechanisms and the properties of mixtures in these systems. Future tests involving the
380 controlled addition of liquid water with varying salinities will be necessary for further
381 application to complex natural systems.

382 **Acknowledgements**

383 The authors thank S. Roberts (LLNL) for assisting with ion chromatography
384 measurements; W. Durham (MIT) for providing the OK#1 sand used in this study; J. Pinkston, S.
385 Kirby, D. Lockner, W. Waite, and A. Hunt (USGS) for helpful discussions, advice, and reviews;
386 J. Lemire (SIO) for help with the cell fabrication and design. Data supporting Figs. 3-6 are
387 available in Supporting Information. Support for this work was provided by DOE contract DE-
388 NT0005668 awarded to S. Constable (SIO), and Interagency Agreement DE-NT0006147
389 between the USGS Gas Hydrate Project and the DOE's Methane Hydrate R&D Program.
390 Prepared by LLNL under contract DE-AC52-07NA27344. The use of trade, product, industry, or
391 firm names in this report is for descriptive purposes only and does not constitute endorsement by
392 the U.S. Geological Survey or the U.S. Government.

393 **References**

394 Archie, G. E. (1942), The electrical resistivity log as an aid in determining some reservoir
395 characteristics, *Trans. Am. Inst. Min. Metall. Pet. Eng., 146*, 54-62.
396 Boswell, R., and Collett, T. (2011), Current Perspectives on Gas Hydrate Resources. *Energy and*
397 *Environmental Sciences,* 4, 1206-1215.

Cha, J.-H., and Y. Seol, (2013), Increasing gas hydrate formation temperature for desalination of high salinity produced water with secondary guests, *ACS Sustainable Chem. Eng.*, *1*(10) pp. 1218-1224.

Collett, T. 2002. Energy resource potential of natural gas hydrate. American Association of Petroleum Geologists Bulletin 86, 1971-1992.

Collett, T. S., and J. W. Ladd (2000), Detection of gas hydrate with downhole logs and assessment of gas hydrate concentrations (saturations) and gas volumes on the Blake Ridge with electrical resistivity log data, *Proc. Ocean Drill. Program, Sci. Results*, *164*, 179-191.

Du Frane W. L., L. A. Stern, K. A. Weitemeyer, S. Constable, J. C. Pinkston, and J. J. Roberts (2011), Electrical properties of polycrystalline methane hydrate, Geophys. Res. Lett., 38, L09313. doi:10.1029/2011GL047243.

Durham, W. B., A. V. Pathare, et al. (2009). "Mobility of icy sand packs, with application to Martian permafrost." Geophys. Res. Lett. 36, L23203, doi: 10.1029/2009GL040392.

Dvorkin, J., M. B. Helgerud, W. F. Waite, S. H. Kirby, and A. Nur, (2000), Introduction to physical properties and elasticity models. In *Natural Gas Hydrate In Oceanic and Permafrost Environments*, edited by M. D. Max., pp. 245–260, Kluwer Academic Publishers, Dordrecht, Netherlands (NLD).

Edwards, R. N. (1997), On the resource evaluation of marine gas hydrate deposits using sea-floor transient electric dipole-dipole methods, *Geophysics*, *62*(1), 63-74.

Ellis, M. H., T. A. Minshull, M. C. Sinha, and A. I. Best (2008), Joint seismic/electrical effective medium modelling of hydrate-bearing marine sediments and an application to the Vancouver Island margin. In: Proceedings of the 6th International Conference on Natural Gas Hydrates.

6th International Conference on Gas Hydrates Vancouver BC, Canada, International Conference on Gas Hydrates, 5586-[12p].

Evans, R. L. (2007), Using CSEM techniques to map the shallow section of seafloor: From the coastline to the edges of the continental slope, *Geophysics*, *72*(2), WA105-WA116.

Glover, P. W. J., M. J. Hole, and J. Pous (2000), A modified Archie's law for two conducting phases, *Earth Planet. Sci. Lett.*, *180*, 369-383.

Hashin, Z., and S. Shtrikman (1962), A variational approach to the theory of effective magnetic permeability of multiphase materials, *J. Appl. Phys.*, *33*, 3125-3131.

Hornbach, M. J., W. S. Holbrook, A. R. Gorman, K. L. Hackwith, D. Lizarralde, and I. Pecher (2003), Direct seismic detection of methane hydrate on the Blake Ridge, *Geophysics*, *68*(1), 92-100.

Kneafsey, T. J., Y. Seol, A. Gupta, and L. Tomutsa (2011), Permeability of laboratory-formed methane-hydrate-bearing sand: measurements and observations using X-ray computed tomography, *SPE Journal*, *16*(1), pp. 78–94.

Kvenvolden, K. A. (1999), Potential effects of gas hydrate on human welfare, *Proc. Natl. Acad. Sci. U. S. A.*, *96*(7), 3420-3426.

Kvenvolden, K., Lorenson, T., 2001. The global occurrence of natural gas hydrate. *In*: Natural gas hydrates: Occurrence, distribution, and detection (Paull C., and Dillon, W., eds.) Geophysical Monograph, 124, 87–98.

Lee, J. Y., J. C. Santamarina, and C. Ruppel (2010), Parametric study of the physical properties of hydrate-bearing sand, silt, and clay sediments: 1. Electromagnetic properties, *J. Geophys. Res., [Solid Earth]*, *115*: B11104, doi:10.1029/2009JB006669.

Li, F. G., C. Y. Sun, S. L. Li, G. J. Chen, X. Q. Guo, L. Y. Yang, H. Pan, S. Li, and K. Zhang (2012), Experimental studies on the evolvement of electrical resistivity during methane hydrate formation in sediments, *Energy Fuels*, 26, 6210-6217.

Maslin, M., M. Owen, R. Betts, S. Day, T. Dunkley Jones, and A. Ridgwell (2010), Gas hydrates: past and future geohazard?, *Proc. R. Soc. A*, *368*(1919), 2369-2393.

Milkov, A. V. (2004), Global estimates of hydrate-bound gas in marine sediments: how much is really out there?, *Earth-Sci. Rev.*, *66*(3-4), 183-197.

Nelson, H., S. Schildmann, A. Nowaczyk, C. Gainaru, B. Geil, and R. Bohmer (2013), Small-angle water reorientations in KOH doped hexagonal ice and clathrate hydrates, *Phys. Chem. Chem. Phys.*, 15, 6355-6367.

NIIR Board of Consultants & Engineers (2005), The Complete Book on Glass and Ceramics Technology, Asia Pacific Business Press, 624 pages.

Petrenko, V. F., and R. W. Whitworth (1999), *Physics of Ice*, Oxford Univ. Press Inc., New York.

Ren, S. R., Y. Liu, and W. Zhang (2010), Acoustic velocity and electrical resistance of hydrate bearing sediments, *J. Petrol. Sci. Eng.*, 70, 52-56.

Revil, A., P. Kessouri, and C. Torres-Verdín (2014), Electrical conductivity, induced polarization, and permeability of the Fontainebleau sandstone, *Geophysics*, 79(5), D301-D318.

Roberts, J. J. (2002), Electrical properties of microporous rock as a function of saturation and electrical conductivity, *J. Appl. Phys.*, *91*(3), 1687-1694.

Roberts, J. J., and J. A. Tyburczy (1991), Frequency-dependent electrical-properties of polycrystalline olivine compacts, *J. Geophys. Res., [Solid Earth]*, *96*(B10), 16205-16222.

Roberts, J. J., and J. A. Tyburczy (1993), Impedance spectroscopy of single and polycrystalline olivine - evidence for grain-boundary transport, *Phys. Chem. Miner.*, *20*(1), 19-26.

Ruppel, C., 2007, Tapping methane hydrates for unconventional natural gas. Elements, 3(3), 193-199.

Schwalenberg, K., E. Willoughby, R. Mir, and R. N. Edwards (2005), Marine gas hydrate electromagnetic signatures in Cascadia and their correlation with seismic blank zones, *First Break*, *23*, 57-63.

Sloan, E. and Koh, C. 2007. Clathrate hydrates of natural gases, 3rd Edition. Taylor & Francis/CRC Press, 721 p.

Spangenberg, E., and J. Kulenkampff (2006), Influence of methane hydrate content on electrical sediment properties, *Geophys. Res. Lett.*, *33*(24).

Stern, L. A., S. H. Kirby, and W. B. Durham (1996), Peculiarities of methane clathrate hydrate formation and solid-state deformation, including possible superheating of water ice, *Science*, *273*(5283), 1843-1848.

Stern, L. A., S. H. Kirby, S. Circone, and W. B. Durham (2004), Scanning electron microscopy investigations of laboratory-grown gas clathrate hydrates formed from melting ice, and comparison to natural hydrates, *Am. Mineral.*, *89*(8-9), 1162-1175.

Stern, L.A., T.D. Lorenson, and J.C. Pinkston (2011), Gas hydrate characterization and grain-scale imaging of recovered cores from the Mount Elbert Gas Hydrate Stratigraphic Test Well, Alaska North Slope, *Marine and Petroleum Geology*, 28, pp. 3940403.

Waite, W. F., L. A. Stern, S. H. Kirby, W. J. Winters, and D. H. Mason (2007), Simultaneous determination of thermal conductivity, thermal diffusivity and specific heat in sI methane hydrate, *Geophysical J. Int.*, *169*(2), 767-774.

Wallmann K., E. Pinero, E. Burwicz, M. Haeckel, C. Hensen, A. Dale, and L. Ruepke (2012), The global inventory of methane hydrate in marine sediments: A theoretical approach. *Energies*, *5*, 2449-2498.

Webb, D. A. (1939), The sodium and potassium content of sea water, *J. Exp. Biol.*, *16*, 178-183.

Weitemeyer, K. A., S. C. Constable, K. W. Key, and J. P. Behrens (2006), First results from a marine controlled-source electromagnetic survey to detect gas hydrates offshore Oregon, *Geophys. Res. Lett.*, *33*(3).

Weitemeyer K. A., S. Constable, and A. M. Tréhu (2011). A marine electromagnetic survey to detect gas hydrate at Hydrate Ridge, Oregon, Geophys. J. Int., doi: 10.1111/j.1365-246X.2011.05105.x.

Wildenschild, D., J. J. Roberts, and E. D. Carlberg (2000). On the relationship between microstructure and electrical and hydraulic properties of sand-clay mixtures, *Geophys. Res. Lett.*, *27*(19), 3085-3088.

Wolery, T. W. (1992), EQ3/6, a software package for geochemical modeling of aqueous systems; UCRL MA-110662-PT-1; Lawrence Livermore National Laboratory: Livermore, CA.

Zhang, Z. J., and G. A. McMechan (2006), Elastic inversion for distribution of gas hydrate, with emphasis on structural controls, *J. Seismic Explor.*, *14*(4), 349-370.

Table1. Summary of sample compositions, run conditions, and Equation (1) fits for parameters σ_0 and E_a.

Sample	H_2O phase	H_2O (vol%[a])	SiO_2 (vol%[a])	T cycles	P (MPa)	Dissoc. T (°C)	Dissoc. t (days)	Log[σ_0 (S/m)]	E_a (kJ/mol)
Run without sediment									
Run 1[b]	Synth. Test	100.0	0.0	n/a	16.9-25.8	n/a	n/a	n/a	n/a
Run 2[b]	hydrate	100.0	0.0	10	18.3-21.3	-15	1	0.965	27.9
	ice	100.0	0.0		0.0			6.63	54.5
Run 3[b]	hydrate	100.0	0.0	7	16.2-18.5	-15	13	1.50	30.6
	ice	100.0	0.0		0.0			5.00	45.5
Runs with OK#1 quartz sand									
Run 5	hydrate	90.0	10.0	8	23.8-26.4	-15	8	1.78	31.3
	ice	88.7	11.3		0.0			5.71	50.7
Run 6	hydrate	70.0	30.0	13	18.2-23.3	-3	11	2.42	33.7
	ice	67.0	33.0		0.0			6.49	50.7
Run 4	hydrate	57.7	42.3	16	21.5-25.7	n/a	n/a	-2.02	7.66
	ice	54.2	45.8		n/a			n/a	n/a
Run 8	hydrate	57.7	42.3	12	20.0-23.4	-3	6	-2.13	6.52
	ice	54.2	45.8		0.0			4.92	41.5
Run 10	hydrate	10.0	90.0	13	20.2-24.3	-3	6	-4.90	-0.503
	ice	8.8	91.2		0.0			-4.24	2.07
Runs with soda-lime-silica beads									
Run 7	hydrate	57.2	42.8	15	6.1-9.1	-3	9	n/a	n/a
	ice	53.8	46.2		0.0			n/a	n/a
Run 9	hydrate	57.7	42.3	7	18.8-22.7	n/a	n/a	0.227	23.4
	ice	54.3	45.7		n/a			n/a	n/a

[a] Excludes porosity.
[b] Data from *Du Frane et al.*, 2011.

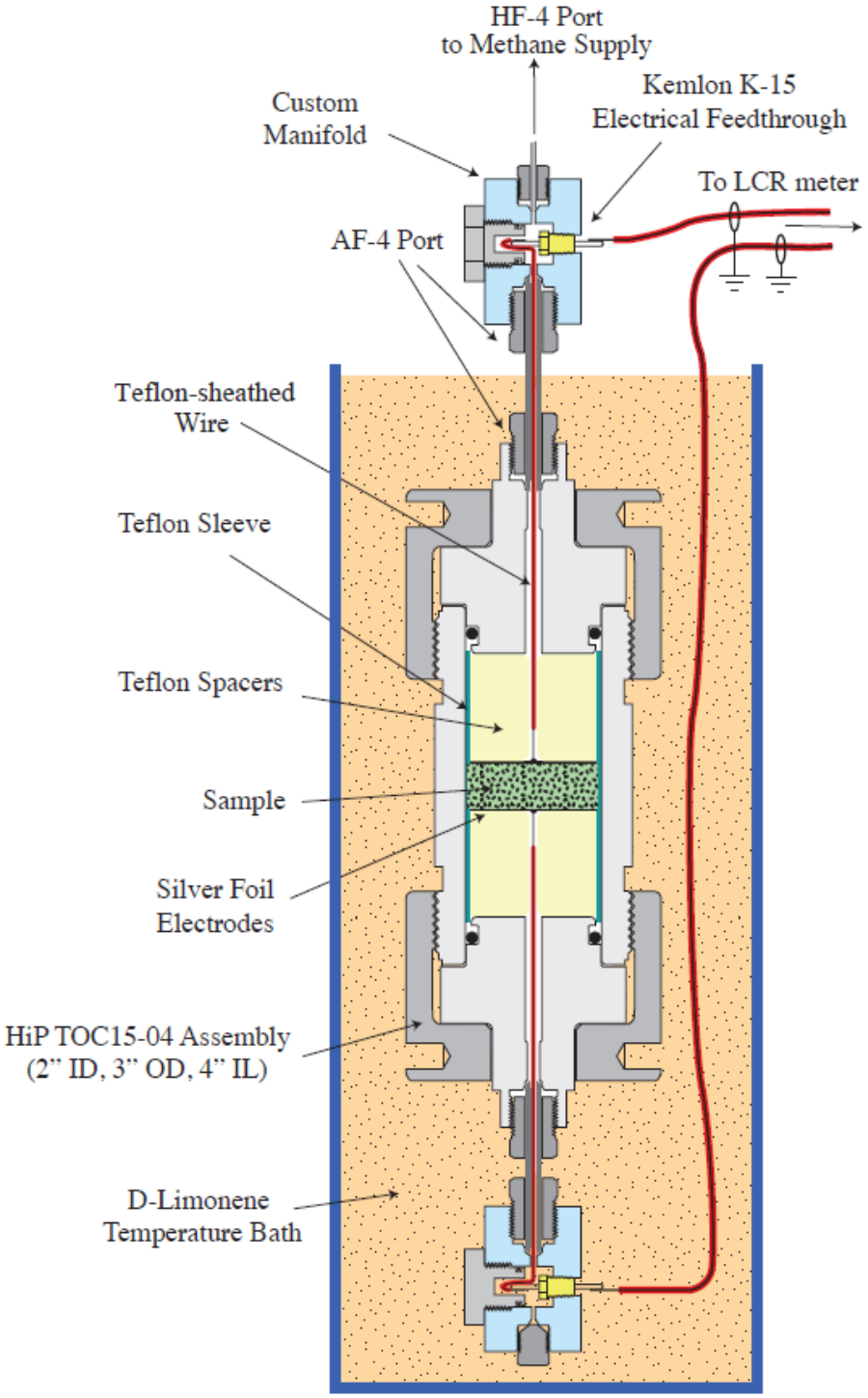

508

509 **Figure 1.** Pressure vessel designed to synthesize gas hydrate and measure impedance

510 spectroscopy *in situ* [from *Du Frane et al.*, 2011].

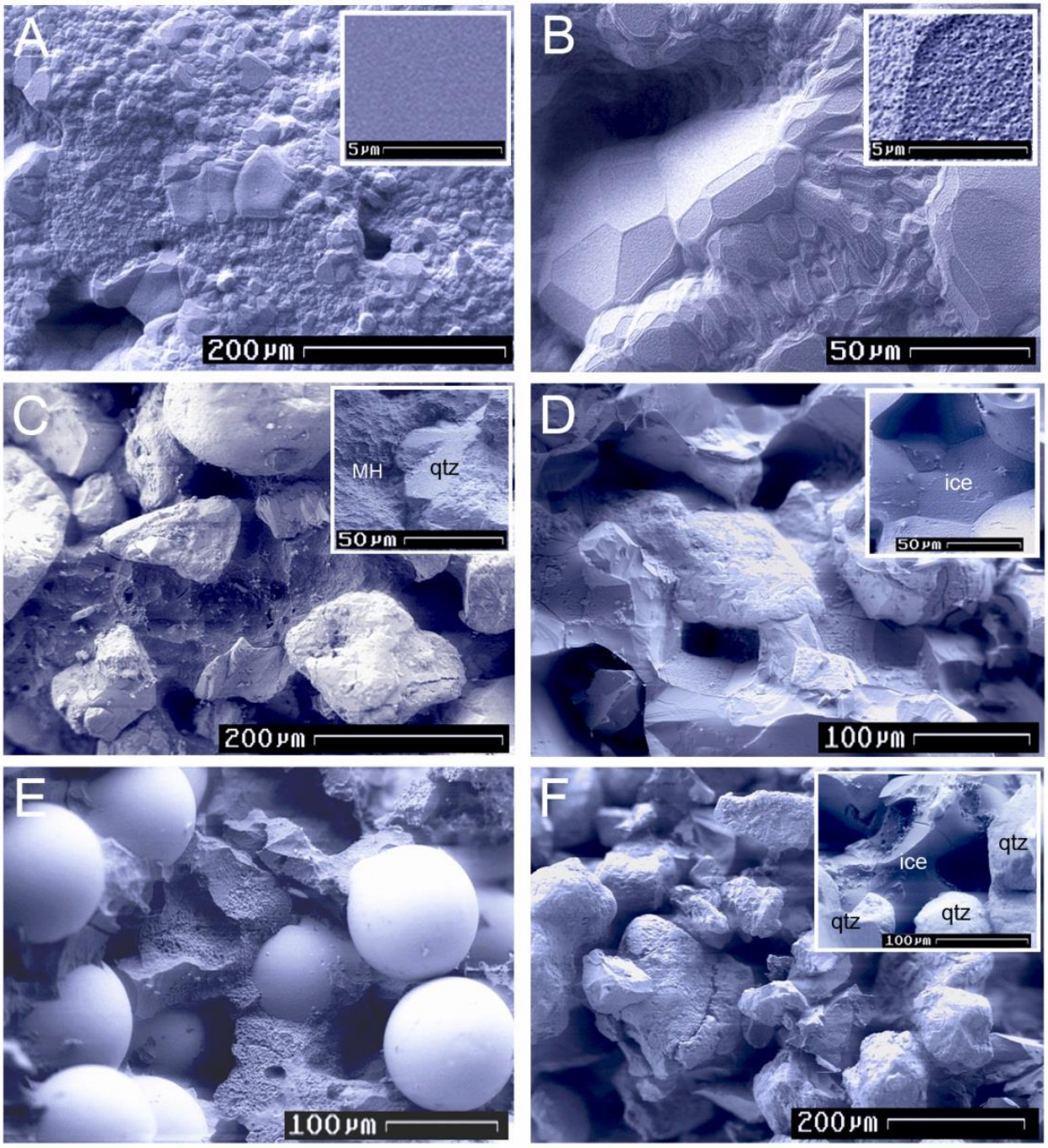
A
5 µm
200 µm
B
5 µm
50 µm
C
MH
qtz
50 µm
200 µm
D
ice
50 µm
100 µm
E
100 µm
F
ice
qtz
qtz
qtz
100 µm
200 µm

511

512

513 **Figure 2.** Cryo-SEM images of CH_4 hydrate and hydrate-sediment mixtures. Single-phase
514 polycrystalline CH_4 hydrate had ~20% porosity, grain size diameters of 10-80 microns, and were
515 fully dense as-grown (A, inset), but developed surface pitting with time in the high-vacuum SEM
516 column, which resulted in a nano- or meso-porous surface texture (B, inset). C shows a
517 ~55:45vol% hydrate:sand sample (Run 4) and D shows a ~55:45vol% ice:sand sample (Run 8).
518 Significant annealing of the ice grains accompanies dissociation at our test conditions (compare
519 D and C insets), but there is no significant migration of sand, thus enabling comparison of
520 measurements before and after dissociation. E shows a 55:45vol% hydrate:beads sample (Run 9).
521 SEM shows uniform distribution of phases in all three samples (C, D, and E) as well as
522 similarities in the nature of the grain contacts, helping establish a basis for comparison of
523 conductivity measurements. The pitting and more porous appearance of 2E is a result of
524 sublimation of gas hydrate under high-vacuum conditions in the FE-SEM column, which is
525 accentuated in samples with higher sediment content due to higher surface-to-volume ratio of the
526 hydrate phase [*Stern et al.*, 2004]. F shows a 10:90vol% ice:sand sample (Run 10), with
527 connecting ice expanded in the inset. In D and F, the samples are more porous than A-C because
528 the hydrate-to-ice dissociation reaction results in a ~16% volumetric reduction of the H_2O phase,
529 as discussed in text.

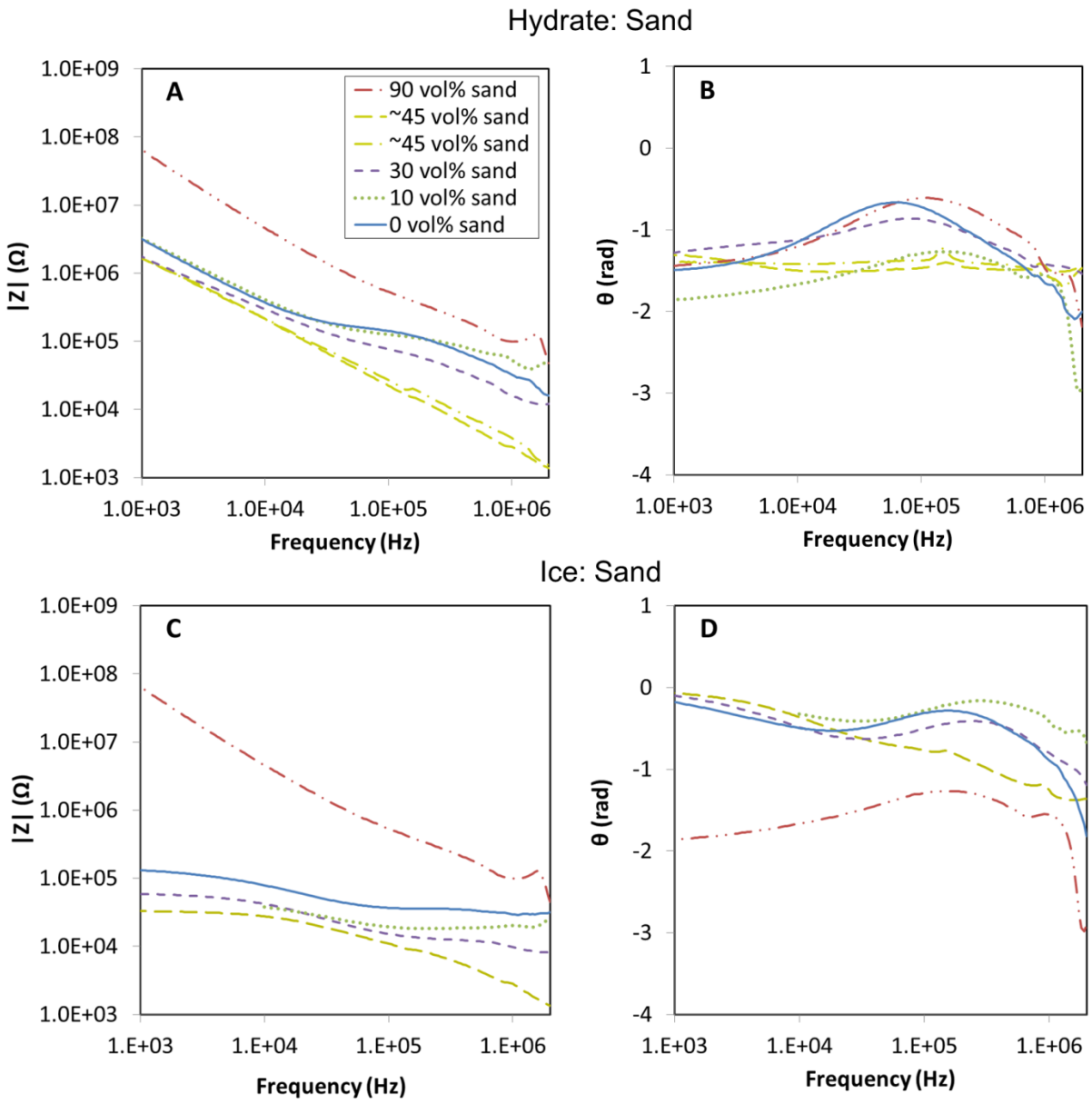

530

531 **Figure 3.** Total impedance magnitude (|Z|) and phase (θ) data as a function of frequency

532 collected for CH_4 hydrate: sand mixtures (A, B), and ice: sand mixtures after dissociation of CH_4

533 (C, D). Data are plotted for CH_4 hydrate/ice without sediment as a solid blue line [*Du Frane et*

534 *al.*, 2011].

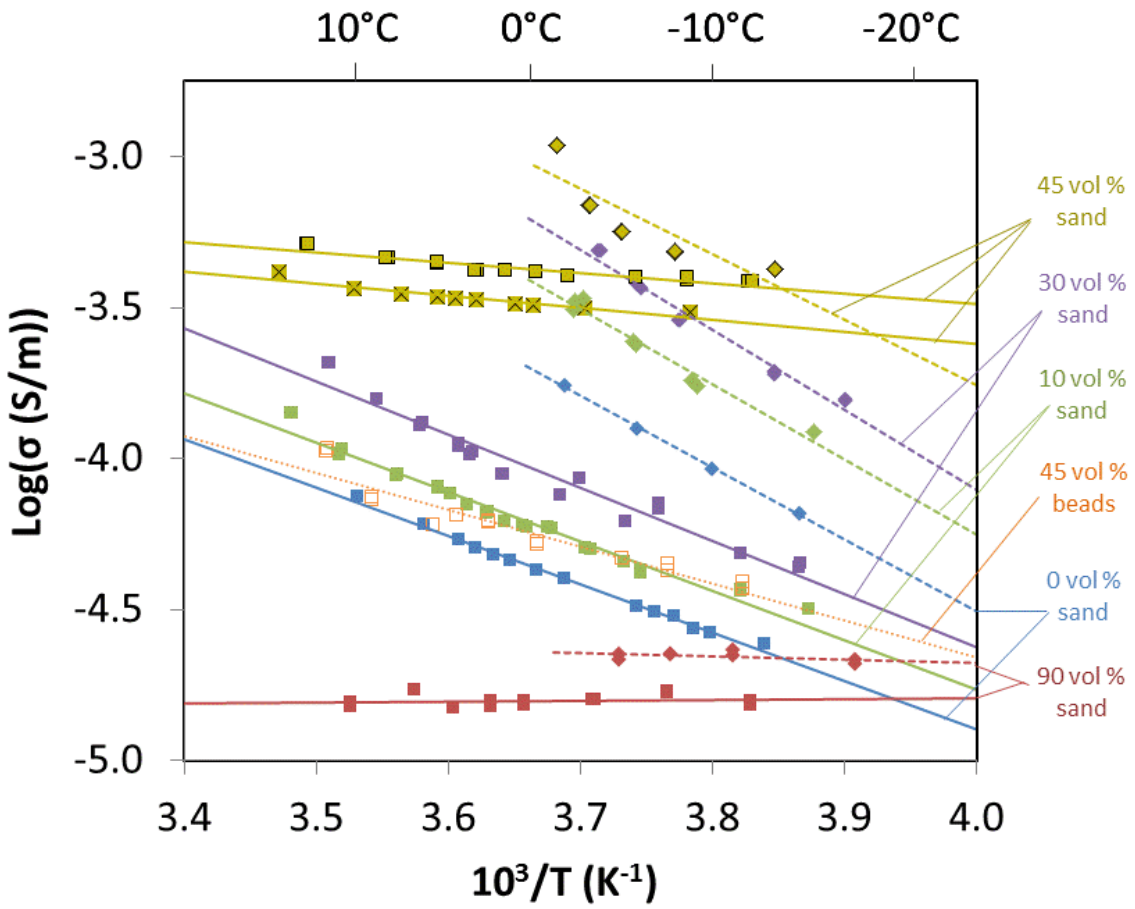

535

536 **Figure 4.** Electrical conductivity measurements versus inverse temperature for CH_4 hydrate in
537 mixtures with sand (closed squares, with fits shown as solid lines) or glass beads (open squares,
538 with fit shown as a dotted line), and ice dissociated from hydrate in mixtures with sand (filled
539 diamonds, with fits shown as dashed lines). Two runs were performed with ~45 vol% sand: run 4
540 is shown as yellow squares with 'X's; run 8 is shown as outlined, yellow squares/diamonds.
541 Linear data-fits to Equation 1 are given in Table 1 with slopes that are proportional to activation
542 energy (E_a) and intercepts equal to $Log(\sigma_0)$.

543

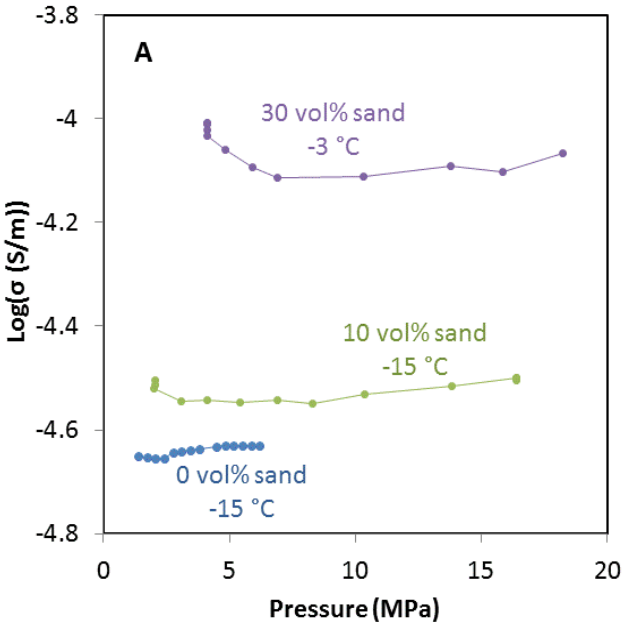

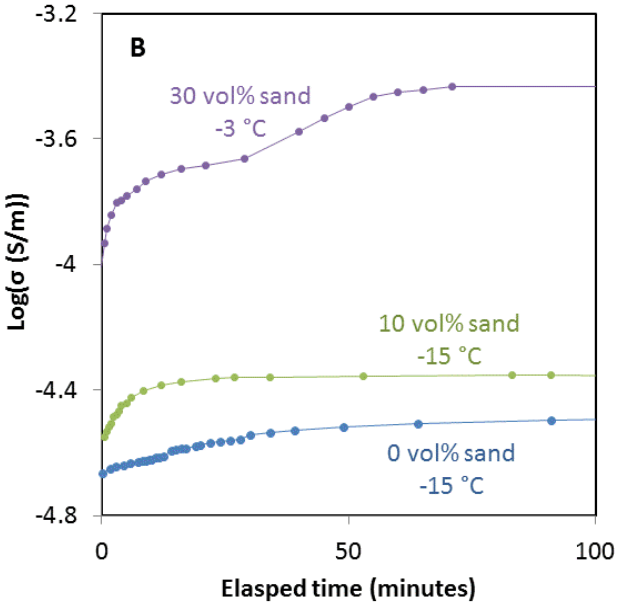

Figure 5. Electrical conductivity of sample mixtures during dissociation of CH_4 hydrate back into ice as a function of pressure (A), and as a function of elapsed time (B). Samples dissociated at a significantly higher rate at -3 °C than at -15 °C.

Supporting Information for

Electrical properties of methane hydrate + sediment mixtures

In Prep. for J. Geophys. Res.

Wyatt L. Du Frane[1], Laura A. Stern[2], Steven Constable[3], Karen A. Weitemeyer[3,4], Megan M. Smith[1], Jeffery J. Roberts[1]

[1]Lawrence Livermore National Laboratory, 7000 East Ave, Livermore, CA, 94550 USA.

[2]U. S. Geological Survey, 345 Middlefield Rd., Menlo Park, CA, 94025 USA.

[3]Scripps Institution of Oceanography, 8622 Kennel Way, La Jolla, CA 92037, USA.

[4]National Oceanography Centre Southampton, University of Southampton Waterfront Campus, European Way, Southampton SO14 3ZH, UK.

Contents of this file

Other files

Data for all figures in the manuscript and Supporting Information are included in a spreadsheet with filename: “Figure data Du Frane et al JGR 2015.xlsx”

Introduction

This document contains sections on S1. Ionic Impurities Analyses and S2. Electrical Conductivity Modeling, with supporting table and figures.

573 ***S1. Ionic Impurities Analyses***

574 The H_2O from the initial seed ice and from 4 run samples (Runs 3, 5, 6, and 7) was
575 melted and extracted to determine what ionic impurities may have been introduced to CH_4
576 hydrate grains from the sediments used in this study (OK#1 sand or glass beads). However, it is
577 important to note that the melting process also rinses off additional materials from the sediments
578 that were not present in the H_2O while it was in the form of CH_4 hydrate or ice. Analyses
579 performed on the H_2O melted from mixed samples (hereafter referred to as 'melt samples') only
580 indicate what ions were present at grain boundaries, not necessarily what was incorporated into
581 the structure of CH_4 hydrate or ice grains. To help address this issue, we also analyzed mixtures
582 of sand (S1-S4) and beads with water to constrain the relative amounts of impurities that may
583 have been rinsed off into melt samples during this processing (hereafter referred to as 'rinse
584 samples', as not to be confused with 'melt samples' obtained from actual gas hydrate synthesis
585 runs).

586 **Methods**

587 The ice remaining after dissociation in post-run samples 3, 5, 6, and 7 was melted and
588 analyzed to determine what impurities were present at grain boundaries. Most of the impurities
589 measured in the water from samples were likely introduced after melting, meaning these
590 measurements only serve to constrain what impurities might have been incorporated into the
591 crystalline structures of gas hydrate or ice grains during experiments. The ice-sediment mixtures
592 were loaded into 60 mL syringes. The ice was melted to water and expelled into vials through
593 Luer lock 0.25 μm filters to separate the water from the sediment. The run 10 sample with 90
594 vol% sand did not produce sufficient liquid for analysis. For comparison, milliQ water

595 (5.6×10^{-3} S/m) was mixed with varying weight ratios (0.5, 1.0, 1.5, 2.0) of glass beads or OK#1
596 sand to determine what impurities are transferred simply by rinsing sediments. After 7 days these
597 'rinse sample' mixtures were loaded into syringes and water was expelled through Luer lock
598 0.25 μm filters into vials. We performed direct current electrical conductivity (σ_{DC})
599 measurements on each of these water samples using an OMEGA PHB-70x Water Analyzer with
600 0.5% accuracy. The instrument was calibrated by 4 commercial standard solutions ranging from
601 10.66 to 2.07×10^{-1} S/m. Smaller volume samples were diluted with 5-12 mL MilliQ water in
602 order to completely submerge the conductivity probe for accurate readings, and were later
603 corrected for dilutions.

604 The water melted from run samples was analyzed to determine ionic concentrations and
605 solution chemistry. Ionic chromatography (IC) was performed using a Metrohm 881.
606 Concentrations of several common anions (fluoride, bromide, chloride, nitrite, nitrate, phosphate,
607 and sulfate) and cations (ammonium, calcium, lithium, magnesium, potassium, sodium) were
608 determined by comparing against calibration standards at several different dilutions. The reagent
609 water used was ASTM Type II distilled, deionized water (18 Mohm) that was free of the anions
610 of interest and particles > 0.20 μm. The eluent used for anions contained 3.2×10^{-3} mol/L of
611 Na_2CO_3 and 1.0×10^{-3} mol/L of $NaHCO_3$. The eluent used for cations contained 0.35 mol/L of
612 $H_2C_2O_4$. The samples were also measured for total inorganic carbon (TIC) using an OI
613 Analytical Aurora 1030. Prior to analyses, samples were stored in air-tight vials, and were not
614 acidified. Analyses were performed at room temperature. The pH was calculated from IC and
615 TIC data by assuming charge balance and using the code EQ3/6 and the data.shy database
616 [*Wolery*, 1992].

617 **Results**

DC electrical conductivity measurements (σ_{DC}) were performed on melt and rinse samples (Table S1, Fig. S1A). The melted seed ice that was used as starting material had a value of 2.20(±0.01) x 10^{-3} S/m. The melt sample without sediment (run 3) was slightly higher in value with σ_{DC} = 1.46(±0.01) x 10^{-2} S/m after melting. Samples with 10 vol% (run 5) and 30 vol% (run 6) of OK#1 sand had significantly higher σ_{DC} values of 4.21(±0.02) x 10^{-2} S/m and 2.63(±0.01) x 10^{-1} S/m respectively. Run 7 contained 45 vol% glass beads (same as run 9) but failed experimentally as it left the CH_4 hydrate stability field during one of the temperature cycles in the synthesis step due to pressure loss. The run 7 sample was still useful for post-run analysis for impurities. This sample had the highest σ_{DC} of 3.45(±0.02) x 10^{-1} S/m. The electrical conductivities of the melt samples were generally higher in comparison to the rinse samples when plotted as a weight ratio of sediment to water (referred to in shorthand as SiO_2:H_2O) (Fig. S1A). The sediment rinse samples had σ_{DC} that exhibited linear relationships with sediment to water weight ratios, indicating that impurities were rinsed off of sediments at amounts that were below saturation. Glass bead rinse samples had σ_{DC} that was 2.5 times higher than sand rinse samples.

IC measurements performed on the rinse and melt samples indicated that Na^+ concentrations had the most similar trend to the relative magnitudes of the σ_{DC} measurements (Figs. S1A and S2A). Glass bead rinse samples had significantly higher Na^+ concentrations than sand rinse samples (Fig. S2A). K^+, Ca^{2+}, and Mg^{2+} were only detected in melt and rinse samples that contained sand (Figs. S2 B-D). The Ca^{2+} and Mg^{2+} quantities were similar between the melt samples and rinse samples, but melt samples contained significantly higher amounts of Na^+ and K^+ than rinse samples for a given amount of sand. Melt samples from all runs exhibited some Cl^- (Fig. S2E) and smaller amounts of SO_4^{2-} (Fig. S2F). The melt sample without sediment (run 3)

had small amounts of both Na and Cl (Table S1) that suggests ~10^{-3} mol/L NaCl was added during experimental handling. The total molar charge measured by IC (meq/L) was positive in all samples (Fig. S1B). Anions CO_3^{2-} and HCO_3^- were not measured by IC, so TIC measurements were performed to constrain their possible concentrations, but do not indicate their aqueous speciation (Fig. S1C). Assuming all major dissolved species that contribute to electrical solution neutrality were accounted for, and remaining charge imbalances is attributed to H+ species, we calculated pH at room temperature using EQ3/6 code (Fig. S1D). These calculations indicate that both the OK#1 sand and glass beads decrease water acidity, which is consistent with measurements performed on diluted samples that had slightly elevated pH.

Discussion

We attempted to constrain what impurities may have been incorporated into the CH_4 hydrate or ice structures from the sand or glass beads by analyzing water melted from run samples (Table S1, Fig. S1 and S2). Unfortunately, these analyses also include any other impurities that were present at grain boundaries, but were excluded from crystallization of the CH_4 hydrate or ice. Impurities have vastly different solubility in liquids versus solids. The effects of impurities on σ are also different. So caution is required in the interpretation of σ_{DC}, IC, and TIC measurements of water melted from samples, as they do not directly pertain to the electrical conductivities that were measured in the samples when the H_2O was CH_4 hydrate or ice.

The electrical conductivities, and some ionic concentrations, were higher in melt samples than in rinse samples (Fig. S1 and Fig. S2). The sample with no sediment (run 3) verifies that relatively few impurities (mostly NaCl) were gained during storage, contact with the experiment apparatus, or handling of samples. Thus, the discrepancy between melt samples and the rinse samples suggests that more ionic impurities were transferred from sediments throughout

experimental runs than what could simply be rinsed off their surfaces. The effects of the freezing and thawing of the H_2O during CH_4 synthesis may have allowed for more efficient chemical interaction with the surfaces of the sand and bead sediments. This could especially be the case for sand, which is likely to have somewhat weathered surfaces containing clays.

Contact with glass beads produced higher electrical conductivity in melt samples (run 7) than contact with sand (Fig. S1A). The σ_{DC} of melt samples appears to be dominated by Na^+ concentrations, because they show similar trends in their relative magnitudes (Fig. S1A and S2A). Na^+ and TIC values were very high in samples that were in contact with glass beads relative to sand. This was likely due to sodium carbonate Na_2CO_3, which is frequently used as flux to reduce silica melting temperature for glass making [*NIIR Board of Consultants & Engineers*, 2005]. The electrical conductivity of CH_4 hydrate-glass beads mixture (run 7) was not significantly higher than pure CH_4 hydrate (run 3) (Fig.4). This indicates that most impurities that were measured in higher concentrations from the surfaces of the glass beads (Na^+, CO_3^{2-}, and HCO_3^-) were likely excluded during CH_4 hydrate formation. Conversely, at least some of the ionic impurities measured in higher concentrations from the surfaces of the sand grains (K^+, Ca^{2+}, Mg^{2+}, NH_4^+, Cl^-, SO_4^{2-}) were included during CH_4 hydrate formation to account for increased electrical conductivity values.

S2. Electrical Conductivity Modeling

In this section we present our first-order attempt to model the doping effect that impurities from sand have on the electrical conductivity of mixtures with CH_4 hydrate. Petrophysical mixing laws can be used to describe the behavior caused by variations in the ratios of hydrate to sand and ice to sand in our sample mixtures. The sample mixtures examined in this study can be divided into 3 regimes: 1. well-connected CH_4 hydrate with poorly-connected sand; 2. well-connected CH_4 hydrate with well-connected sand; 3. poorly-connected CH_4 hydrate with well-connected sand. This is similarly the case for ice-sand mixtures after CH_4 dissociation. Essentially, there are two percolation thresholds (one for each phase within sample mixtures) that must be considered. There are numerous petrophysical mixing laws [e.g., *Glover et al.*, 2000], but none adequately express mixing behaviors across percolation thresholds. This requires that each regime be modeled individually. Our limited data coverage limits us to modeling the first regime.

Building the model

First we assume that gas hydrate is the primary conduction path for current in our sample mixtures (see main text for supporting arguments), and that the electrical conductivity of the sand is low enough to be negligible. SEM images indicate that mixtures are generally homogenous throughout all samples. In this case a simple parallel mixing model is sufficient for describing the total electrical conductivity through well-connected phases:

$$\sigma(\text{mixture}) = \sigma(\text{hydrate})*\text{vol\%(hydrate)} + \sigma(\text{sand})*\text{vol\%(sand)} \quad \text{(S1)}$$

where σ is the total electrical conductivity and vol% is the volume percentage for CH_4 and sand respectively. The sand is not well-connected necessarily, but if $\sigma(\text{sand}) << \sigma(\text{hydrate})$ then the second term would approximately be equal to zero anyway:

$$\sigma(\text{mixture}) = \sigma(\text{hydrate})*\text{vol\%(hydrate)} \quad \text{(S2)}$$

Similar equations can be assumed for the ice after dissociation. The electrical conductivity of pure CH_4 hydrate and resulting ice after dissociation was measured by *Du Frane et al.* [2011]

$$\sigma(\text{pure hydrate}) = 10^{1.50}(\text{S/m})e^{-30.6(\text{kJ/mol})/RT} \quad \text{(S3)}$$

$$\sigma(\text{pure ice}) = 10^{5.00}(\text{S/m})e^{-45.5(\text{kJ/mol})/RT} \quad \text{(S4)}$$

We use these measurements to constrain the model at 0 vol% sand. To model the doping effect that impurities in sand have on gas hydrate and ice we add a second conductivity term, σ(doping). The concentration of impurities that can be transferred from the surfaces of the sand grains, and thus this second conductivity term, will increase proportionally with the volume percentage of sand

$$\sigma(\text{doping}) = \sigma_0(\text{doping})*e^{-Ea(\text{doping})/RT}*\text{vol\%(sand)} \quad \text{(S5)}$$

The combining this with measurements on pure hydrate or ice total conductivity becomes

$$\sigma(\text{hydrate}) = \sigma(\text{pure hydrate}) + \sigma(\text{doping}) \quad \text{(S6)}$$

$$\sigma(\text{ice}) = \sigma(\text{pure ice}) + \sigma(\text{doping}) \quad \text{(S7)}$$

Combining these expressions gives us our fit equations for data collected on sand mixtures with both CH_4 hydrate and ice

$$\sigma(\text{hydrate-sand mixture}) = \{10^{1.50}(\text{S/m})e^{-30.6(\text{kJ/mol})/RT} + \mathbf{\sigma_0(doping)}*e^{-\mathbf{Ea(doping)}/RT}*\text{vol\%(sand)}\}*\text{vol\%(hydrate)} \quad \text{(S8)}$$

$$\sigma(\text{ice-sand mixture}) = \{10^{1.50}(\text{S/m})e^{-45.5(\text{kJ/mol})/RT} + \mathbf{\sigma_0(doping)}*e^{-\mathbf{Ea(doping)}/RT}*\text{vol\%(sand)}\}*\text{vol\%(ice)} \quad \text{(S9)}$$

where σ_0(doping) and Ea(doping) are the only variables used to fit data. Fits were determined using least squares regression analysis.

Fitting results and discussion

Only a portion of the data set could be fit to equations S8 and S9 due to changes in connectivity of the hydrate and sand phases in mixtures as concentrations were varied. The fitting equations are based on a simple parallel mixing law that assumes at least the conducting phases are well connected. This works for certain concentrations of CH_4 hydrate/ice to sand, but cannot be extended to concentrations where significant changes occur in connectivity of conductive phases or mechanisms. Our data set includes sample mixtures with 0, 10, 30, ~45, 90 vol% sand. Multiple fits were attempted including data for increasing volume percentages of sand. Only data for mixtures with < 45 vol% sand could be satisfactorily fit simultaneously to the same solution for both ice and gas hydrate. The solutions were as follows:

$$\sigma(\text{hydrate-sand mixture}) = \{10^{1.50}(\text{S/m})e^{-30.6(\text{kJ/mol})/RT} + \mathbf{10^{3.65}}(\text{S/m})e^{-\mathbf{37.6}(\text{kJ/mol})/RT} * \text{vol\%(sand)}\} * \text{vol\%(hydrate)} \quad \text{(S10)}$$

$$\sigma(\text{ice-sand mixture}) = \{10^{1.50}(\text{S/m})e^{-45.5(\text{kJ/mol})/RT} + \mathbf{10^{4.95}}(\text{S/m})e^{-\mathbf{40.1}(\text{kJ/mol})/RT} * \text{vol\%(sand)}\} * \text{vol\%(ice)} \quad \text{(S11)}$$

These solutions are in excellent agreement with data for 0 (by definition), 10 and 30 vol% sand for mixtures with both CH_4 hydrate and ice that were included in the fit, but as expected are in poor agreement with data for ~45 or 90 vol% sand that were excluded from the fit (Fig. S3).

The data for ~45 vol% data has a significantly different behavior with larger increase in electrical conductivity at lower temperatures and less overall temperature dependence. The repeatability of this trend in a second experiment gives us high confidence in the accuracy of the observed trends. The substantial change in overall activation energy suggests a change in primary conduction mechanism for these mixtures. For this ratio both CH_4 hydrate and sand are well connected, as evidenced by SEM images (i.e. second data regime). The electrical conductivity data for ~90 vol% is low magnitude and has a very little temperature dependence.

750 Also SEM images of this sample mixture indicate the CH_4 hydrate is poorly connected and the
751 sand is well connected (i.e. third data regime).
752 Electrical conductivity is highest when both sand and hydrate are connected. Although
753 the gas hydrate still appears to be the primary conduction path throughout these mixtures, as
754 evidenced by the very low electrical conductivity of 90 vol% sand data. This would seem to
755 indicate that the actual interfaces between hydrate/ice and sand may be more conductive than the
756 bulk conductivity of hydrate/ice grains, particularly at the lower temperatures in the measured
757 range. The electrical conductivity of mixtures with 45 vol% sand may be dominated by
758 connected interfaces between hydrate/ice and sand.

Table S1. Ion chromatography analyses.

	SiO_2:H_2O	Cl^-	NO_3^-	SO_4^{2-}	F^-	Br^-	PO_4^{3-}	NO_2^-	Na^+	K^+	Ca^{2+}	Mg^{2+}	Li^+	NH_4^+
	(wt ratio)	(mol/L)	(mol/L)	(mol/L)	(mol/L)	(mol/L)	(mol/L)	(mol/L)	(mol/L)	(mol/L)	(mol/L)	(mol/L)	(mol/L)	(mol/L)
Melt samples														
Seed Ice	0.00	8.84E-05	*8.84E-06*	1.12E-05	n.d.	n.d.	n.d.	n.d.	1.42E-04	*2.01E-05*	*5.86E-07*	n.d.	n.d.	n.d.
Run 3	0.00	1.01E-03	*1.24E-05*	1.58E-05	*6.21E-06*	n.d.	n.d.	n.d.	7.96E-04	*1.95E-05*	*6.35E-06*	*8.97E-06*	n.d.	3.39E-04
Run 5	0.37	2.08E-03	*4.26E-05*	4.32E-04	*8.20E-06*	n.d.	n.d.	n.d.	2.85E-03	*1.32E-04*	*1.40E-04*	*2.08E-04*	n.d.	2.28E-04
Run 6	1.43	1.59E-02	*1.74E-04*	2.30E-03	*3.16E-06*	n.d.	n.d.	n.d.	2.07E-02	*5.32E-04*	*6.77E-04*	*9.37E-04*	n.d.	8.75E-04
Run 7	2.48	4.59E-03	*2.39E-04*	5.80E-04	*2.45E-04*	n.d.	n.d.	n.d.	3.70E-02	*6.78E-05*	n.d.	n.d.	n.d.	n.d.
Rinse samples mixed with sand														
S1	0.50	2.42E-04	*3.99E-05*	4.24E-04	n.d.	n.d.	n.d.	n.d.	9.68E-04	1.16E-04	2.19E-04	3.16E-04	n.d.	n.d.
S2	1.00	4.73E-04	*2.79E-05*	9.63E-04	*4.96E-07*	*1.12E-05*	n.d.	*2.95E-05*	1.70E-03	2.08E-04	4.46E-04	6.68E-04	n.d.	n.d.
S3	1.51	6.43E-04	*2.73E-05*	1.28E-03	n.d.	*1.70E-05*	n.d.	*1.54E-05*	2.30E-03	2.77E-04	6.29E-04	8.38E-04	n.d.	*5.13E-05*
S4	2.01	9.65E-04	*2.80E-05*	1.76E-03	n.d.	*1.96E-05*	n.d.	*1.56E-05*	3.21E-03	3.65E-04	7.99E-04	1.05E-03	n.d.	*8.85E-05*
Rinse samples mixed with glass beads														
B1	0.50	*1.79E-05*	*1.43E-05*	4.98E-05	*9.85E-06*	n.d.	n.d.	n.d.	5.72E-03	*5.38E-06*	*7.61E-05*	1.66E-04	n.d.	n.d.
B2	1.00	*2.70E-05*	*1.56E-05*	8.03E-05	*2.54E-05*	n.d.	n.d.	n.d.	1.06E-02	*8.18E-06*	*8.01E-05*	1.33E-04	n.d.	n.d.
B3	1.51	*3.59E-05*	*1.80E-05*	1.19E-04	*3.82E-05*	n.d.	n.d.	n.d.	1.53E-02	*8.35E-06*	*8.58E-05*	1.13E-04	n.d.	n.d.
B4	2.01	*5.30E-05*	*3.01E-05*	1.56E-04	*5.13E-05*	n.d.	n.d.	n.d.	2.02E-02	*1.63E-05*	*1.17E-04*	*9.57E-05*	n.d.	n.d.

Italics indicate raw measurement values below calibration standards.
n.d. (not detected) indicates concentrations below detection limit.

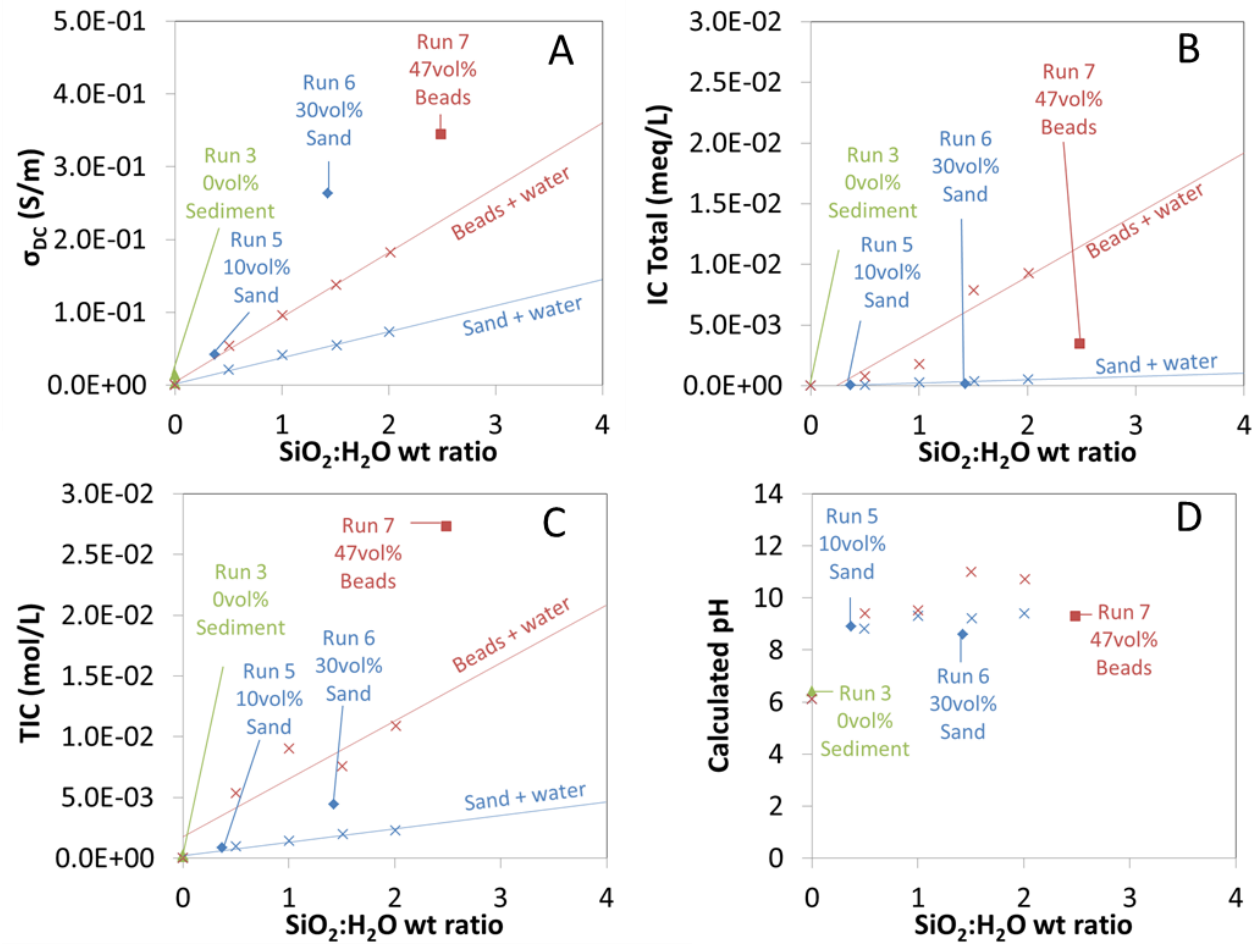

Figure S1. A) Direct current conductivity, B) Total charge detected by ion chromatography (complete results in Table S1), C) total inorganic carbon, D) calculated pH (using EQ3/6) as a function of weight ratio of quartz sand or silica beads (SiO_2) to water (H_2O) in melted run samples and sediment rinse samples. Run 3 without sediment is shown as a green triangle, runs 5 and 6 with sand as blue diamonds, and run 7 with beads as a red square. Sediment rinse samples are shown as blue 'X's for sand (S1-S4) and red 'X's for beads (B1-B4) with linear fits in corresponding colors.

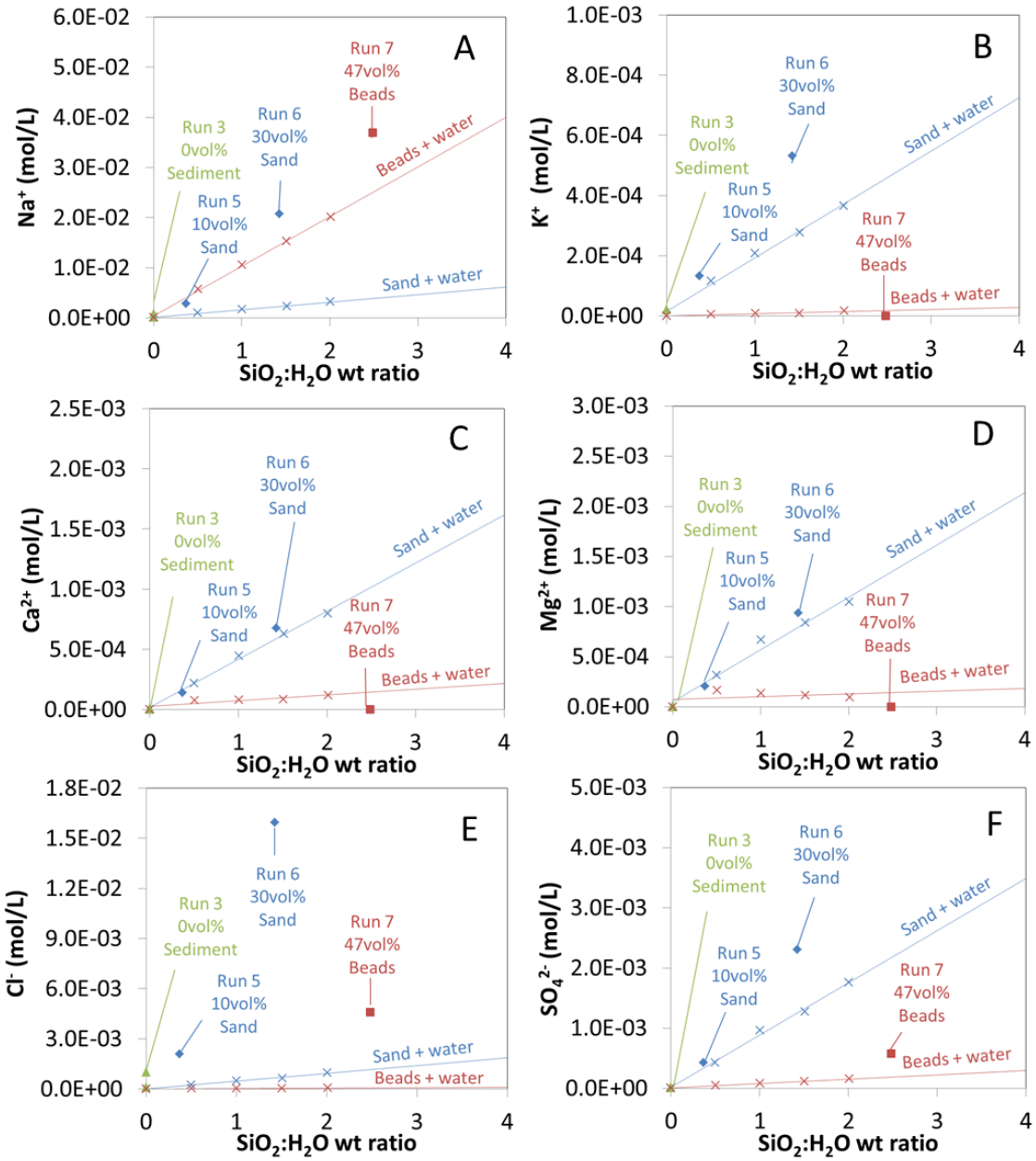

Figure S2. A-F) Ionic concentrations as a function of weight ratio of quartz sand or silica beads (SiO_2) to water (H_2O) in melted run samples and sediment rinse samples (Complete results in Table S1). Run 3 without sediment is shown as a green triangle, runs 5 and 6 with sand as blue diamonds, and run 7 with beads as a red square. Sediment rinse samples are shown as blue 'X's for sand and red 'X's for beads with linear fits in corresponding colors.

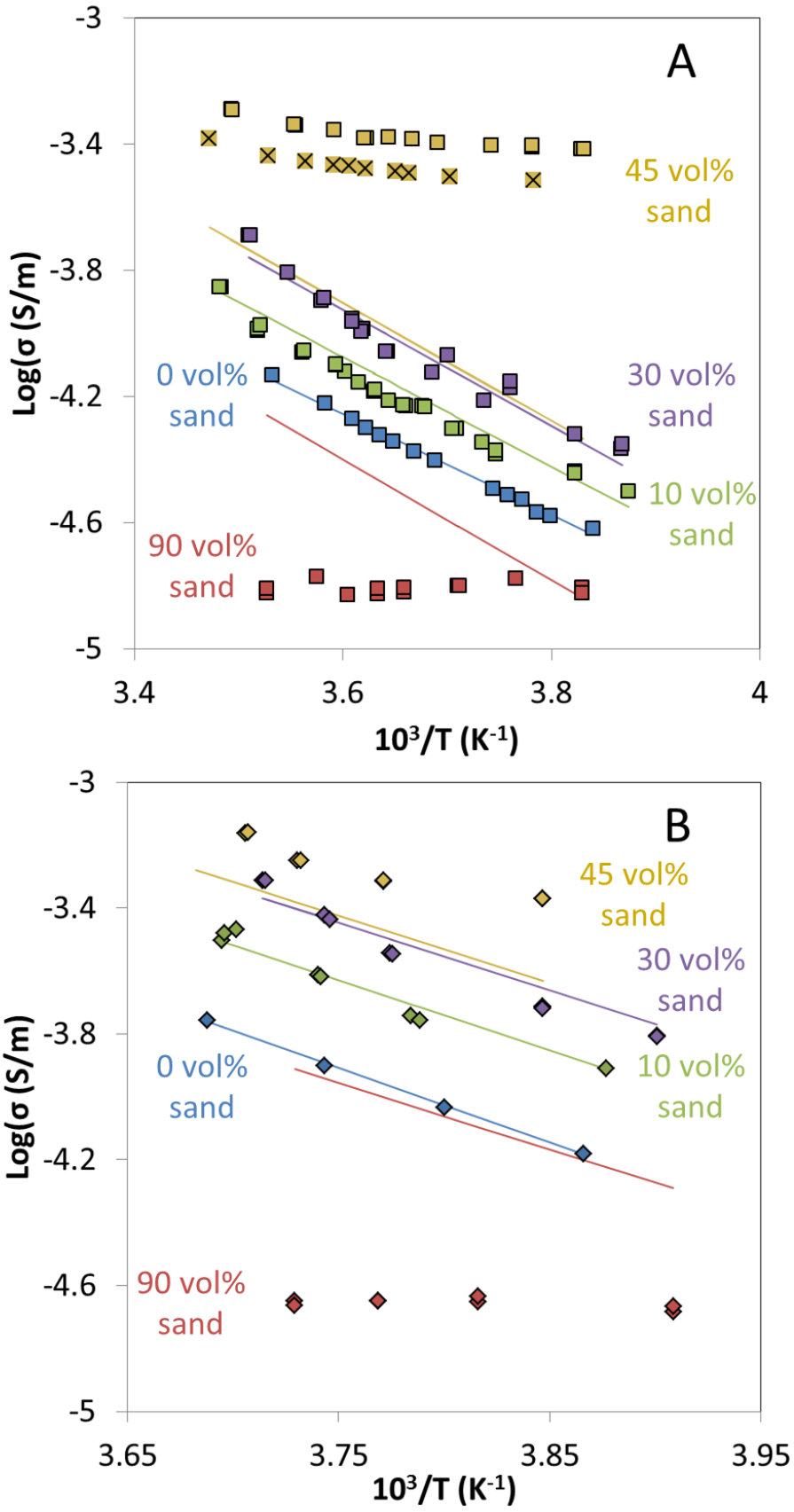
A
45 vol% sand
30 vol% sand
10 vol% sand
0 vol% sand
90 vol% sand
Log(σ (S/m)
-3
-3.4
-3.8
-4.2
-4.6
-5
3.4
3.6
3.8
4
10³/T (K⁻¹)
B
45 vol% sand
30 vol% sand
10 vol% sand
0 vol% sand
90 vol% sand
Log(σ (S/m)
-3
-3.4
-3.8
-4.2
-4.6
-5
3.65
3.75
3.85
3.95
10³/T (K⁻¹)

777

778 **Figure S3.** Electrical conductivity model of doping effect caused by impurities from sand in
779 mixtures with A) CH_4 hydrate and B) ice after dissociation. Samples with 0 vol% sand are shown
780 in blue, 10 vol% in green, 30 vol% in purple, ~45vol% in yellow, 90 vol% in red. Data fits
781 (Equations S10 and S11) are shown as lines with the same corresponding colors. Fitting included
782 data for mixtures with 0, 10, and 30 vol% sand, and excluded data for 45 and 90 vol% sand.